

Joint Resource Management for Energy-efficient UAV-assisted SWIPT-MEC: A Deep Reinforcement Learning Approach

Yue Chen, Hui Kang, Jiahui Li, Geng Sun, *Senior Member, IEEE*, Boxiong Wang, Jiacheng Wang, Cong Liang, Shuang Liang, and Dusit Niyato, *Fellow, IEEE*

Abstract—The integration of simultaneous wireless information and power transfer (SWIPT) technology in 6G Internet of Things (IoT) networks faces significant challenges in remote areas and disaster scenarios where ground infrastructure is unavailable. This paper proposes a novel unmanned aerial vehicle (UAV)-assisted mobile edge computing (MEC) system enhanced by directional antennas to provide both computational resources and energy support for ground IoT terminals. However, such systems require multiple trade-off policies to balance UAV energy consumption, terminal battery levels, and computational resource allocation under various constraints, including limited UAV battery capacity, non-linear energy harvesting characteristics, and dynamic task arrivals. To address these challenges comprehensively, we formulate a bi-objective optimization problem that simultaneously considers system energy efficiency and terminal battery sustainability. We then reformulate this non-convex problem with a hybrid solution space as a Markov decision process (MDP) and propose an improved soft actor-critic (SAC) algorithm with an action simplification mechanism to enhance its convergence and generalization capabilities. Simulation results have demonstrated that our proposed approach outperforms various baselines in different scenarios, achieving efficient energy management while maintaining high computational performance. Furthermore, our method shows strong generalization ability across different scenarios, particularly in complex environments, validating the effectiveness of our designed boundary penalty and charging reward mechanisms.

Index Terms—UAV-assisted SWIPT-MEC network, DRL, task offloading, resource management, trajectory planning.

I. INTRODUCTION

THE simultaneous wireless information and power transfer (SWIPT) has emerged as a promising technology for Internet of Things (IoT) applications in sixth-generation (6G) wireless networks [1]–[4]. The anticipated rapid expansion of IoT networks, characterized by large-scale deployment, automation, and low power consumption [5], [6], presents significant challenges in providing a reliable power supply and network connectivity. Specifically, traditional approaches such as wired connections and battery replacements incur substantial maintenance costs [7], particularly problematic given the increasing computational demands of IoT terminals requiring continuous network connectivity. To address these challenges, SWIPT enables simultaneous energy and information transmission via radio frequency (RF) signals from ground-based stations. However, this solution exhibits limitations in remote areas or disaster scenarios where ground infrastructure is unavailable or damaged, potentially compromising network coverage and communication performance.

Low-altitude unmanned aerial vehicles (UAV) emerge as an effective solution to challenges in traditional IoT networks and SWIPT implementation. Functioning as mobile base stations, UAVs offer cost-effectiveness, mobility, and ease of deployment [8], [9], which attributes are critical for dynamic IoT environments. Their ability to adjust position in real-time establishes line-of-sight (LoS) connections with ground IoT terminals, enhancing wireless network performance and robustness [10]. Additionally, UAVs equipped with mobile edge computing (MEC) servers bring computational resources closer to resource-constrained IoT terminals, reducing processing latency and improving operational efficiency [11], [12]. By simultaneously supporting SWIPT and MEC functionalities, UAVs effectively address both energy harvesting (EH) and computational demands in dynamic and resource-constrained IoT environments.

However, integrating MEC and SWIPT into UAV-assisted 6G-enabled IoT networks while efficiently managing computational tasks presents several challenges [13]–[15]. *First*, UAVs face inherent energy limitations due to battery size and weight constraints [16], which necessitate efficient energy allocations for movement, communication, and computation.

This work is supported in part by the National Natural Science Foundation of China (62172186, 62272194, 62471200), in part by the Science and Technology Development Plan Project of Jilin Province (20240302079GX, 20250102210JC), in part by the Postdoctoral Fellowship Program of China Postdoctoral Science Foundation (GZC20240592), in part by the China Postdoctoral Science Foundation General Fund (2024M761123), and in part by the Scientific Research Project of Jilin Provincial Department of Education (JJKH20250117KJ). (*Corresponding authors: Jiahui Li and Geng Sun.*)

Yue Chen, Hui Kang, Jiahui Li, and Boxiong Wang are with the College of Computer Science and Technology, Jilin University, Changchun 130012, China. Hui Kang is also with the Key Laboratory of Symbolic Computation and Knowledge Engineering of Ministry of Education, Jilin University, Changchun 130012, China. (E-mails: yuechen23@mails.jlu.edu.cn; kanghui@jlu.edu.cn; lijiahui@jlu.edu.cn; wangbx0320@163.com).

Geng Sun is with the College of Computer Science and Technology, Jilin University, Changchun 130012, China, and also with the Key Laboratory of Symbolic Computation and Knowledge Engineering of Ministry of Education, Jilin University, Changchun 130012, China. He is also with the College of Computing and Data Science, Nanyang Technological University, Singapore 639798 (E-mail: sungeng@jlu.edu.cn).

Jiacheng Wang and Dusit Niyato are with the College of Computing and Data Science, Nanyang Technological University, Singapore (E-mails: jiacheng.wang@ntu.edu.sg; dniyato@ntu.edu.sg).

Cong Liang is with China Mobile Communications Group Jilin Co., Ltd. (E-mails: liangcong@jl.chinamobile.com).

Shuang Liang is with the School of Information Science and Technology, Northeast Normal University, Changchun 130117, China (E-mails: liangshuang@nenu.edu.cn).

In particular, the decision variables of UAV flight strategy, such as velocity, have a nonlinear relationship with propulsion power consumption, thus further posing optimization difficulty [17]. *Second*, the limited computational resources and communication bandwidth of UAVs may be insufficient to meet the computational and energy demands of multiple IoT devices simultaneously [18], which means that the energy charging fairness among these IoT devices must be considered. *Third*, stochastic task arrivals and channel condition fluctuations bring dynamics to the considered UAV-assisted multi-terminal SWIPT-MEC network, causing the static optimization method to lack adaptability [19], [20].

To address these challenges comprehensively, we formulate a bi-objective optimization problem related to the total energy consumption of the system and the average battery level of the terminals in a UAV-assisted multi-terminal SWIPT-MEC system. The main contributions of this paper are summarized as follows:

- *UAV-assisted Multi-terminal SWIPT-MEC System with directional antenna*: We consider a novel UAV-assisted network that integrates SWIPT with MEC support for multiple terminals, specifically designed for regions without coverage from ground base stations. In this system, the UAV functions as a mobile base station providing MEC services while simultaneously employing SWIPT to deliver wireless charging support to terminals. Simultaneously, we consider the UAV with directional antennas to enhance the downlink transmission signal quality. It will improve both communication efficiency and charging capabilities, which ultimately extends the average battery runtime of terminals.
- *Formulation of a Bi-objective Optimization Problem*: We formulate a bi-objective optimization problem, aiming to minimize the total energy consumption of the system and maximize the average battery level of the terminals while ensuring charging fairness among terminals simultaneously. The formulated problem is a non-convex mixed-integer nonlinear programming problem with a hybrid solution space, i.e., discrete and continuous variables.
- *DRL-base Solution*: We propose a novel deep reinforcement learning (DRL)-based off-policy optimization approach. We first reformulate the optimization problem as a Markov decision process (MDP). Subsequently, we design an action simplification mechanism to address the hybrid action space. Based on this, we propose an improved soft actor-critic (SAC) algorithm that enhances the processing and modeling capabilities of neural networks, thereby resulting in superior convergence performance.
- *Performance Evaluation and Analysis*: Simulation results demonstrate that the proposed algorithm outperforms various baselines across key metrics, yielding a 47.86% improvement in average terminal retained energy and a 65.15% enhancement in charging fairness. Moreover, the proposed algorithm exhibits fast convergence and effectively learns the maximum entropy optimal policy, successfully balancing exploration and exploitation in complex decision spaces. Furthermore, it demonstrates

strong generalization capabilities across diverse terminal distributions, particularly in the case of uneven distribution.

The rest of this paper is organized as follows. Section II reviews the related research activities. Section III presents the directional antenna-enhanced UAV-assisted multi-terminal SWIPT-MEC network and optimization problem formulation. Section IV proposes our DRL-based solution. Simulation results are presented and analyzed in Section V. Finally, this work is concluded in Section VI.

II. RELATED WORK

In this section, we review related works on paradigms, optimization objectives, and optimization methods in UAV-assisted SWIPT-MEC networks.

A. Paradigms in MEC Networks

MEC technology allows computation-intensive and latency-critical applications to be offloaded from resource-constrained mobile devices to proximate network edges [21], which attracts considerable research interest. The related literature on MEC networks can be classified into three distinct research paradigms.

Ground MEC Networks: Offloading computational tasks from mobile devices to ground-based stations represents the foundational paradigm of MEC. For example, the authors in [22] proposed an Internet of Video Things (IoVT) network based on MEC, combined with the reconfigurable intelligent surface (RIS). However, ground-based MEC systems face significant challenges related to scalability and disaster recovery capabilities. In remote areas, these systems often become inoperative due to insufficient base station coverage and inadequate infrastructure support.

UAV-assisted MEC Networks: The integration of UAVs effectively addresses critical limitations of traditional ground MEC networks by deploying UAVs as mobile base stations or communication relays. For instance, the authors in [23] utilized a UAV as either an MEC server or wireless relay within a UAV-assisted MEC system. While these contributions advance UAV-assisted MEC capabilities, they overlooked the energy requirements of mobile terminals, which are particularly crucial for energy-constrained devices such as sensors.

UAV-assisted WPT-MEC Networks: Some studies have now applied wireless power transmission (WPT) technology, utilizing UAVs as power sources to charge mobile devices. The authors in [24] investigated a UAV-assisted WPT-MEC system, where the UAV provided both power and computation services to mobile terminals.

Despite advances in the field, research remains limited on utilizing UAVs to simultaneously provide charging and downlink information transmission services for terminals in MEC networks. This capability is particularly valuable in areas lacking ground-based infrastructure and better aligns with practical implementation demands.

B. Optimization Objectives in UAV-assisted Networks with WPT/SWIPT

In the paradigms of UAV-assisted WPT/SWIPT networks, common optimization objectives are typically categorized into the following two main aspects.

Energy-related Objectives: Several studies focus on energy-related objectives, such as energy consumption and energy efficiency (EE). For example, the authors in [25] proposed a novel time division multiple access (TDMA)-based workflow model, aiming to minimize the total energy consumption of the UAV. Likewise, the authors in [26] formulated an optimization problem in the scenario of a UAV-enabled wireless-powered cooperative MEC system, seeking to minimize the total required energy of the UAV. The authors in [3] investigated the EE maximization optimization problem for device-to-device (D2D) communications underlying UAVs-assisted industrial IoT networks with SWIPT. Nonetheless, the aforementioned studies concentrate on the energy consumption or EE of UAVs or systems, without considering optimization objectives related to the performance of ground terminals.

Terminals-related Objectives: Several studies focus on the objectives related to terminal performance. For instance, the authors in [27] considered a heterogeneous MEC system with multiple energy-limited IoT devices and a UAV to maximize the minimum task computation data volume among all active devices. Similarly, the authors in [28] integrated SWIPT-enabled non-orthogonal multiple access (NOMA) with a UAV, aiming to maximize achievable rates for the ground users. The authors in [29] considered a UAV-assisted SWIPT system to maximize the sum of the logarithmic average throughput of the GNs. However, the aforementioned research emphasizes the terminal-related metrics but neglects the overall system performance optimization.

As a result, we construct a directional antenna-enhanced UAV-assisted multi-terminal SWIPT-MEC system. In contrast to existing studies, our approach targets optimization objectives at two levels. At the macro level, we aim to minimize UAV energy consumption, while at the micro level, our objective is to maximize the battery energy of the terminals, ensuring charging fairness among the terminals.

C. Optimization Methods in UAV-assisted Networks with WPT/SWIPT

To achieve the aforementioned optimization objectives, various methods have been employed in the literature, which can be broadly categorized into the following categories.

Convex optimization methods: Several studies use traditional static convex or non-convex optimization methods. For example, the authors in [30] investigated a UAV-assisted SWIPT network and proposed a convex optimization method that combines successive convex approximation (SCA) and a quadratic transformation approach. However, convex optimization methods have limitations in terms of applicability and global convergence, especially in weakly constrained problems involving complex structures and multiple local optima.

Evolutionary Computation Methods: Several studies employ evolutionary computation methods to address non-convex optimization problems due to the coupled variables. For instance,

the authors in [31] proposed a multi-objective evolutionary algorithm based on decomposition (MOEA/D) for an emergency communication framework in UAV-enabled SWIPT IoT networks. However, evolutionary computation methods are prone to being trapped in local optima when confronted with high-dimensional data and multimodal problems, and their performance is often highly sensitive to parameter settings.

Traditional DRL Methods: More recently, some studies have attempted to utilize conventional DRL methods to solve dynamic nonlinear programming problems and address the complexities of dynamic environments to achieve enhanced system performance. Specifically, the authors in [32] considered a computation-intensive MEC network based on NOMA-SWIPT and proposed a multi-agent deep deterministic policy gradient (MADDPG)-based resource management algorithm. The authors in [33] studied an energy-efficient UAV network enhanced by RIS with SWIPT, maximizing the average EE by employing the deep Q-learning (DQL) framework. However, the aforementioned works do not offer targeted improvements to address the complexities and variability of dynamic environments.

In summary, distinct from prior studies, we propose a novel DRL-based method for directional antenna-enhanced UAV-assisted multi-terminal SWIPT-MEC systems. This approach effectively tackles dynamic task offloading and UAV scheduling challenges while addressing high-dimensional action-state spaces with a low-complexity solution. Consequently, our method achieves an optimal strategy that balances competing optimization objectives.

III. SYSTEM MODEL AND PROBLEM FORMULATION

In this section, we introduce a directional antenna-enhanced UAV-assisted multi-terminal SWIPT-MEC system with details presented as follows.

Fig. 1 illustrates our proposed system comprising fixed ground IoT terminals, denoted as $i \in \mathcal{I} = \{1, \dots, I\}$. These terminals need to perform computational tasks and transfer information simultaneously for applications such as water quality detection, fire warning, and humidity monitoring. However, in remote areas, the absence of available ground infrastructure makes it impossible to directly provide service to these terminals [19]. Moreover, these terminals are inherently constrained by their limited computational resources and battery capacity, which significantly restricts their task-processing capabilities and service lifetimes.

To address these challenges, we deploy a UAV u equipped with a directional antenna to provide communication, computing services, and energy supply through SWIPT technology [34]. Note that we consider one UAV for the sake of simplicity, and the proposed model can be further extended to multi-UAV cases. Specifically, we first divide the network into clusters using algorithms such as k-means and then apply our modeling approach to each cluster independently.

Fig. 2 illustrates our discrete-time model that partitions continuous time into T discrete equal-duration time slots. Specifically, we define the collection of time slots as $\mathcal{T} = \{1, \dots, t, \dots, T\}$, and the duration of each time slot is denoted

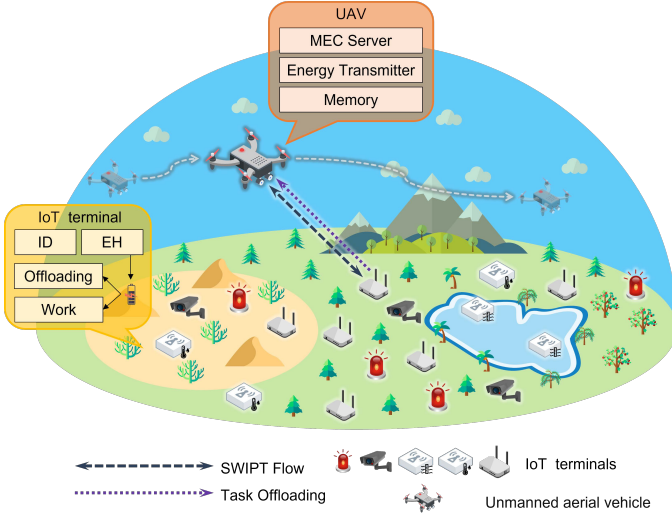


Fig. 1. The directional antenna-enhanced UAV-assisted multi-terminal SWIPT-MEC system.

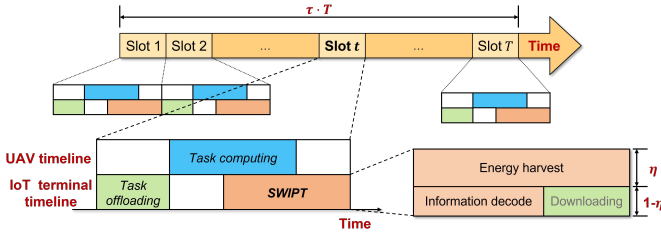


Fig. 2. The time slot division model in the offloading scenario.

as τ , which is chosen to be sufficiently small such that each time slot maintains quasi-static conditions. Thus, we consider that the channel state information (CSI) and the position of the UAV remain constant within a single time slot [4]. When an IoT terminal i offloads its task to the UAV for processing, each time slot is composed of the following phases:

- **Task Offloading Phase:** The IoT terminal offloads its computing task to the UAV.
- **SWIPT and Computation Phase:** After receiving the task, the UAV processes it and transmits the signal to the terminal via a directional antenna. These signals simultaneously deliver both information (external data and computation results) and energy to the terminal. The terminal then performs signal splitting to enable both information decoding (ID) and EH.

Without loss of generality, we denote the coordinates of the ground IoT terminal i as $p_i = (x_i, y_i, 0)$. The UAV operates at a fixed altitude H [3], [4], with its position at time slot t represented as $p_u^t = (x_u^t, y_u^t, H)$.

A. Task Model

In this section, we describe the task generation model and the associated offloading decision-making process.

For the downlink communication, terminal i receives information data $D_{i,r}$ from the UAV, which possesses sufficient storage capacity to carry all required information.

For the uplink communication, computational tasks at IoT terminal i arrive according to a Bernoulli process during

time slot t [35], generating either 0 or 1 task in a time slot. Each task is characterized by a tuple $\{D_{i,p}^t, t_{\text{gen}}, C_i\}$, where $D_{i,p}^t$ represents the data size of task (bit), t_{gen} indicates the generation time slot, and C_i denotes the computation intensity (cycles/bit). We consider these computational tasks to be atomic, requiring completion within a single time slot. Consequently, only two processing strategies are available: local computation or complete offloading to the UAV [36]. This approach allows complex tasks comprising multiple indivisible units to be treated as separate atomic tasks, enhancing problem tractability.

To effectively describe task processing strategies of terminal i , we define a binary indicator $o_i^t \in \{0, 1\}$ representing the offloading decision in time slot t , where $o_i^t = 1$ indicates task offloading and $o_i^t = 0$ represents local processing. The selection of o_i^t depends on the size of the task and processing requirements, as well as current communication conditions and resource availability. As illustrated in Fig. 2, the time slot division model can be expressed as follows:

$$\tau_{\text{up}} + \tau_{\text{S}} \leq \tau, \quad (1)$$

where $\tau_{\text{up}} = \frac{o_i^t(D_{i,p}^t + \delta_{i \rightarrow u})}{R_{i \rightarrow u}}$ represents the task offloading time. The SWIPT time τ_{S} is calculated as the maximum of UAV computing time, EH time, and ID time: $\tau_{\text{S}} = \max \left\{ \frac{o_i^t C_i D_{i,p}^t}{f_u}, \min \left(\frac{E_{\text{max}} - E_i}{E_{u \rightarrow i}}, \tau - \tau_{\text{up}} \right), \frac{D_{i,r} + \delta_{u \rightarrow i}}{R_{u \rightarrow i}} \right\}$. Here, f_u is the CPU frequency (cycles/s) of the UAV, $\delta_{i \rightarrow u}$ and $\delta_{u \rightarrow i}$ are the protocol overheads required for uplink and downlink, respectively. Additionally, E_{max} represents the maximum battery capacity, E_i denotes the remaining battery level of terminal i , while $E_{u \rightarrow i}$ and $R_{u \rightarrow i}$ represent the EH rate and achievable downlink data rate, respectively, which will be detailed in the next section.

B. SWIPT Model

In this part, we introduce the SWIPT model, including the air-to-ground channel models and the non-linear EH model.

1) **Air-to-ground Channel Model:** We employ a probabilistic LoS channel model for communication, where the LoS probability P_{LoS} is given by [37]: $P_{\text{LoS}} = \frac{1}{1 + a_1 \exp\left(-b_1 \left(\frac{180}{\pi} \arctan\left(\frac{H}{d_i^t}\right) - a_1\right)\right)}$. Here, parameters a_1 and b_1 are environment-dependent, H represents the UAV altitude, and d_i^t denotes the horizontal distance between the UAV and terminal i at time slot t , which is calculated as $d_i^t = \sqrt{(x_u^t - x_i)^2 + (y_u^t - y_i)^2}$.

Based on P_{LoS} , the path loss between the UAV and terminal i for a given time slot t can be expressed as follows:

$$L_i^t = 20 \log_{10} \left(\frac{4\pi f_c \|p_u^t, p_i\|}{c} \right) + P_{\text{LoS}} \eta_{\text{LoS}} + (1 - P_{\text{LoS}}) \eta_{\text{NLoS}}, \quad (2)$$

where $\|\cdot\|$ denotes the Euclidean norm, f_c is the carrier frequency, and c is the speed of light. The terms η_{LoS} and η_{NLoS} represent the additional losses associated with LoS and NLoS links, respectively, which are derived from free-space path loss and depend on specific environmental conditions. Consequently, the corresponding channel gain can then be calculated as $h_i^t = 10^{-L_i^t/10}$

Furthermore, to mitigate the impact of channel fading on transmission performance, we consider that the UAV is equipped with a directional antenna, similar to [34], [38]. Accordingly, the antenna gain can be expressed approximately as follows:

$$G_i^t = \begin{cases} \frac{2.28}{\beta^2}, & d_i^t \leq H \tan(\beta) \\ 0, & \text{otherwise} \end{cases}. \quad (3)$$

where β represents the half-power beamwidth (rad) of the antenna.

In the SWIPT communication framework based on the aforementioned model, PS technology is employed to perform both ID and EH simultaneously. In this case, terminal i divides the received RF signal according to PS ratio η , allocating a fraction $(1 - \eta)$ for ID and the remaining fraction η for EH. Therefore, given the total transmit power of the UAV P_{tran} , the signal-to-noise ratio (SNR) at the terminal i can be calculated as follows:

$$\gamma_i = \frac{(1 - \eta)h_i^t P_{\text{tran}} G_i^t}{\sigma^2}, \quad (4)$$

where σ^2 denotes the power of the Gaussian white noise.

Therefore, according to the Shannon theorem, the achievable data rate for terminal i receiving the information of the UAV is given as follows:

$$R_{u \rightarrow i} = B \log_2(1 + \gamma_i), \quad (5)$$

where B denotes the total bandwidth. Conversely, when terminal i transmits to the UAV, the achievable data rate is expressed as:

$$R_{i \rightarrow u} = B \log_2 \left(1 + \frac{P_i h_i^t G_i^t}{\sigma^2} \right), \quad (6)$$

where P_i represents the transmit power of terminal i .

2) *Non-linear EH Model*: For accurate calculation of terminals' EH rates, we adopt a non-linear EH model based on the Logistic function to characterize energy transmission from UAV to terminal. This model represents actual EH circuit characteristics more precisely than linear models. Specifically, the non-linear EH model is formulated as [39]:

$$\mathbb{F}(P_{in}) = \frac{\frac{P_{max}}{1+e^{-a_2(P_{in}-b_2)}} - \frac{P_{max}}{1+e^{a_2 b_2}}}{1 - \frac{1}{1+e^{a_2 b_2}}}, \quad (7)$$

where $\mathbb{F}(P_{in})$ represents the harvested energy under input power P_{in} , the maximum harvested power is denoted as P_{max} , and constant parameters a_2 and b_2 determine the non-linear characteristics related to circuit resistance, capacitance, and diode forward voltage.

In summary, the achievable EH rate can be calculated as follows:

$$E_{u \rightarrow i}(t) = \mathbb{F}(\eta P_{\text{tran}} h_i^t G_i^t). \quad (8)$$

C. Computation Model

Within the proposed system, tasks are executed either via local computation or edge computing during their generation time slot.

If the task is executed locally: Specifically, we consider that the CPU frequency of the terminal i , denoted as f_i , is sufficient to process tasks within a given time slot. In this context, any task generated by terminal i satisfies the

constraint $C_i D_{i,p}^t \leq \tau f_i$. Consequently, similar to [19], the computational energy consumption of the terminal i for a single task can be expressed as follows:

$$E_{i-com}(t) = P_{i-com} \cdot \frac{(1 - o_i^t) C_i D_{i,p}^t}{f_i}, \quad (9)$$

where the computational power of the terminal is represented as $P_{i-com} = k(f_i)^\nu$ [40], where k is the effective capacitance coefficient, and ν is a constant. However, when the remaining energy is very low, the terminal may not have enough energy to process the task. To ensure that the terminal has enough energy to maintain normal operation after processing the task, we define a constraint as follows:

$$E_{i-com}(t) < E_i(t) - (E_{min} + \delta_e), \forall i \in \mathcal{I}, t \in \mathcal{T}, \quad (10)$$

where δ_e represents the reserved energy of a terminal to avoid excessively low energy levels after computation.

If the task is offloaded to the UAV: With the CPU frequency f_u (cycle/s) of the UAV, the computation energy consumption over flight time T is given as follows:

$$E_{u-com}^T = P_{u-com} \sum_{t=1}^T \sum_{i=1}^I \frac{o_i^t C_i D_{i,p}^t}{f_u}, \quad (11)$$

where the computational power of the UAV $P_{u-com} = k(f_u)^\nu$.

D. Energy Consumption Model

In this section, we present the energy consumption models for both the UAV and IoT terminals.

1) *UAV Energy Consumption*: The total energy consumption of the UAV comprises three main components, which can be calculated as follows:

$$E_{uav}^T = E_{u-move}^T + E_{u-tran}^T + E_{u-com}^T, \quad (12)$$

where the first component E_{u-move}^T denotes propulsion energy, calculated as in [41]. Note that E_{u-move}^T varies quadratically with flight velocity, thereby making flight strategy optimization critical for energy efficiency.

The second component E_{u-tran}^T represents the communication energy consumption, which encompasses the energy associated with ID and EH processes. With transmit power P_{tran} , this component at time T is expressed as: $E_{u-tran}^T = P_{\text{tran}} \sum_{t=1}^T \max \left\{ \frac{D_{i,r} + \delta_{u \rightarrow i}}{R_{u \rightarrow i}}, \min \left\{ \frac{E_{max} - E_i}{E_{u \rightarrow i}}, \tau - \tau_{up} \right\} \right\}$. Note that the transmission time in each slot t is determined by the concurrent execution of ID and EH processes.

The third component E_{u-com}^T represents the computation energy consumption, calculated according to Eq. (11).

2) *Terminal Energy Consumption*: The terminal energy consumption can be calculated as follows:

$$E_{terminal}^T = \sum_{t=1}^T \sum_{i=1}^I (E_{i-com}(t) + E_{i-tran}(t)), \quad (13)$$

where the first component $E_{i-com}(t)$ represents the computational energy consumption of terminal i , calculated according to Eq. (9).

The second component $E_{i-tran}(t)$, the transmission energy consumption, is incurred when task $\{D_{i,p}^t, t_{gen}, F_i\}$ is offloaded. In this case, terminal i utilizes a portion of its local storage energy for uplink data transmission. As indicated by Eq. (1), the offloading time is τ_{up} with terminal transmit power

P_i , resulting in $E_{i-tran}(t) = P_i \cdot \tau_{up}$. Note that in each time slot, only one type of energy consumption (either $E_{i-com}(t)$ or $E_{i-tran}(t)$) is incurred, depending on whether $o_i^t = 0$ or $o_i^t = 1$, respectively. Additionally, similar to Eq. (10), $E_{i-tran}(t)$ should satisfy the following constraint:

$$E_{i-tran}(t) < E_i(t) - (E_{min} + \delta_e), \forall i \in \mathcal{I}, t \in \mathcal{T}. \quad (14)$$

Moreover, the terminals need to operate the daily tasks such as monitoring and sensing, which may consume some energy. According to [42], this energy decreases linearly over time. As such, terminal battery energy decreases during daily operations at a rate of ΔE_1 and increases during charging periods at a rate of ΔE_2 . Let E_{min} be the minimum energy threshold for normal terminal operation, and then the energy of terminal i at time slot $t + 1$ can be expressed as follows:

$$E_i(t+1) = \text{clip}(E_i(t) - \Delta E_1 + \Delta E_2, E_{min}, E_{max}), \quad (15)$$

where the function $\text{clip}(*_1, *_2, *_3) = \max(*_2, \min(*_1, *_3))$ ensures that terminal energy remains within the permissible range $[E_{min}, E_{max}]$.

E. Problem Formulation

The considered system concerns two objectives, which are minimizing total energy consumption while maximizing the average battery level of terminals, with an emphasis on ensuring equitable charging distribution among terminals with SWIPT. The key components of these objectives are analyzed as follows:

- 1) Energy consumption is primarily attributed to the UAV propulsion energy E_{u-move}^T and UAV communication energy E_{u-tran}^T , both of which are significantly influenced by flight trajectory and task offloading decisions.
- 2) Enhancing the average battery energy of terminals requires optimization of the achievable EH rate $E_{u \rightarrow i}(t)$. According to Eq. (8), this rate is predominantly determined by the channel gain h_i^t and antenna gain G_i^t , which can be optimized through controlling UAV position.
- 3) Charging fairness among terminals necessitates careful consideration of the terminal charging sequence, which is directly related to flight trajectory planning of the UAV.

To achieve these objectives, we aim to achieve our objectives by optimizing task offloading decisions (O) and UAV trajectory planning, which is decomposed into velocity (\mathbf{v}) and direction (θ). Specifically, we jointly consider the following decision variables:

- 1) $\mathbf{v} = \{v(t) \mid v(t) \in \mathcal{V}^t, t \in \mathcal{T}\}$, a vector consisting of continuous values that denotes the velocity of the UAV movement at each time slot.
- 2) $\theta = \{\theta(t) \mid \theta(t) \in \vartheta^t, t \in \mathcal{T}\}$, a vector consisting of continuous variables, denotes the angle of the UAV movement at each time slot.
- 3) $\mathbf{O} = \{o_i^t \mid o_i^t \in \mathcal{O}^t, i \in \mathcal{I}, t \in \mathcal{T}\}$, a vector consisting of discrete variables, denotes the task offloading decisions of the terminals.

Based on the above analyses, we aim to address the following optimization objectives simultaneously.

Optimization Objective 1: Minimize the total system energy consumption, formulated as follows:

$$E_{total}^T = E_{uav}^T + E_{terminal}^T, \quad (16)$$

where E_{uav}^T and $E_{terminal}^T$ are calculated using Eq. (12) and Eq. (13), respectively.

Optimization Objective 2: Maximize average terminal battery energy while ensuring charging fairness in SWIPT, expressed as follows:

$$F_{energy}(t) = J(t) \cdot \frac{\sum_{i=1}^I E_i(t)}{I}, \quad (17)$$

where $J(t)$ represents Jain's fairness index [43], quantifying the energy distribution among terminals:

$$J(t) = \frac{\left(\sum_{i=1}^I E_i(t)\right)^2}{I \cdot \sum_{i=1}^I (E_i(t))^2}, \quad (18)$$

where the $J(t)$ value approaching 1 indicates more equitable resource allocation across terminals.

In summary, considering the above objectives, we formulate the optimization problem as follows:

$$\mathbf{P}: \min_{\mathbf{v}, \theta, \mathbf{O}} \sum_t E_{total}(t) + \max_{\mathbf{v}, \theta, \mathbf{O}} \sum_t F_{energy}(t) \quad (19a)$$

$$\text{s.t. } p_u^0 = (0, 0), \quad (19b)$$

$$0 < \eta \leq 1, \quad (19c)$$

$$E_{min} \leq E_i(t) \leq E_{max}, \forall i \in \mathcal{I}, t \in \mathcal{I}, \quad (19d)$$

$$\frac{(1 - o_i^t) C_i D_{i,p}^t}{f_i} + o_i^t (\tau_{up} + \tau_S) \leq \tau, \forall i \in \mathcal{I}, t \in \mathcal{I}, \quad (19e)$$

$$R_{min} \leq \min \{R_{u \rightarrow i}, R_{i \rightarrow u}\}, \forall i \in \mathcal{I}, \quad (19f)$$

$$0 \leq v(t) \leq v_{max}, \forall t \in \mathcal{T}, \quad (19g)$$

$$0 \leq \theta(t) \leq 2\pi, \forall t \in \mathcal{T}, \quad (19h)$$

$$C_i D_{i,p}^t \leq \tau f_i, \forall i \in \mathcal{I}, \quad (19i)$$

$$(10), (14). \quad (19j)$$

where v_{max} represents the maximum flight velocity of the UAV, and R_{min} denotes the minimum required communication rate. The constraints ensure system feasibility: Constraint (19b) fixes the initial position of the UAV. Constraint (19c) restricts the power splitting ratio η in SWIPT between 0 and 1. Constraint (19d) maintains terminal battery energy within normal bounds $[E_{min}, E_{max}]$. Constraint (19e) limits the combined local computation and task offloading time to within one time slot. Constraint (19f) guarantees that both uplink and downlink communication rates exceed the minimum threshold. Constraint (19g) and Constraint (19h) regulate the flight velocity and direction of the UAV. Constraint (19i) ensures terminals possess sufficient computational capacity to process tasks within the allocated time frame. Moreover, since optimization problem P consists of two optimization objectives with different units, where E_{total} represents system energy consumption (J) and F_{energy} denotes terminal battery energy (μJ) weighted by the Jain fairness index, we employ a normalized reward function to address unit inconsistency. The optimization problem is further solved using a DRL-based approach.

IV. DRL-BASED METHOD

In this section, we propose a DRL-based offline method to solve the formulated optimization problem. We begin by discussing the motivations for using DRL. Next, we reformulate the optimization problem within an MDP framework. Finally, we detail our proposed method, emphasizing its specific enhancements and comparative advantages for the application domain.

A. Motivations of Using DRL

The problem **(P)** exhibits three distinct properties. First, the scenario under consideration involves a hybrid action space for the UAV, comprising discrete variables (task offloading decisions) and continuous variables (velocity and direction). This hybrid nature renders the formulated problem non-convex. Second, it involves two conflicting objectives. Specifically, reducing $E_{total}(t)$ requires minimizing UAV communication and movement, which consequently decreases energy received at terminals; conversely, improving $F_{energy}(t)$ necessitates more frequent charging and increased flight distances of the UAV, thereby raising energy consumption. Third, the problem encompasses dynamics and uncertainties. The mobility of the UAV dynamically alters both the system network topology and the relative UAV-terminal distances, thereby affecting communication link quality. Additionally, uncertainty arises from the dynamic arrival of terminal tasks, as the UAV possesses limited knowledge of current terminal statuses and environmental conditions, preventing accurate prediction of future offloading task arrivals and processing requirements.

Therefore, the problem **(P)** constitutes a non-convex mixed-integer nonlinear programming problem with conflicting bi-objective optimization that incorporates dynamics and uncertainties. Consequently, traditional optimization methods prove unsuitable for two primary reasons. First, traditional static optimization methods, such as convex or non-convex optimization, struggle to effectively address the highly dynamic and unpredictable nature of this problem [44]. Second, evolutionary computation algorithms (*e.g.*, particle swarm optimization) tend to converge to local optima in complex environments, thereby resulting in suboptimal performance [45].

Consequently, we employ DRL-based methods to solve the optimization problem **(P)** due to their superior robustness and adaptability in dynamic and uncertain environments. This approach provides a more flexible and effective solution for UAV trajectory and resource scheduling.

B. MDP Formulation

To adapt our optimization problem to the DRL-based approach, we first introduce the MDP to model the decision-making process of the UAV (*i.e.*, the agent) [46], [47]. Specifically, an MDP is typically defined by the quintuple $\langle \mathcal{S}, \mathcal{A}, \mathcal{P}, \mathcal{R}, \gamma \rangle$, where \mathcal{S} , \mathcal{A} , $\mathcal{P} = P(s'|s, a)$, $\mathcal{R} = r(a, s)$, and $\gamma \in [0, 1]$ denote state space, action space, state transition probability, reward function, and discount factor, respectively. In this quintuple, the emphasis is on the components \mathcal{S} , \mathcal{A} , and \mathcal{R} , which are critical to our implementation.

State Space: We consider that both the UAV and all terminals employ precise global positioning systems for real-time position tracking. Additionally, since terminals remain stationary, state transitions are represented solely by UAV position changes. Excluding other unobservable factors (*e.g.*, terminal battery levels), we define state s_t as follows:

$$s_t = \{x_u^t, y_u^t\}, t \in \mathcal{T}. \quad (20)$$

This two-dimensional continuous state space simplifies training while maintaining real-world applicability.

Action Space: As outlined in the problem **(P)**, our MDP action space corresponds directly to the decision variables. In each time slot, the UAV needs to determine the offloading decisions for all terminals ($\mathcal{O}^t = \{o_i^t\}, i \in \mathcal{I}$) and movement parameters (velocity v^t and angle θ^t). Correspondingly, the action a_t is defined as follows:

$$a_t = \{\mathcal{O}^t, v^t, \theta^t\}, t \in \mathcal{T}, \quad (21)$$

This hybrid action space, comprising $|\mathcal{I}|$ discrete variables (\mathcal{O}^t) and two continuous variables (v^t and θ^t), substantially increases learning complexity and necessitates careful policy network design in our optimization algorithm.

According to [48], the flight action of the UAV is defined as velocity and angle (v, θ) (rather than Cartesian coordinates (x, y, z)), which effectively captures the temporal dynamics of UAV movement. This approach facilitates practical implementation as it aligns with real-world UAV control commands. Furthermore, this scheme simplifies the action space while enhancing learning efficiency.

Reward Function: The reward function $r(t)$ is crucial for the convergence of DRL algorithms. To enhance stability and generalization capability, we carefully design the reward function $r(t)$ with three components, which are optimization objectives, constraints, and some behavioral incentives. In this study, we aim to minimize the total system energy consumption and maximize average terminal battery energy while ensuring charging fairness. Due to the unit inconsistency, we normalize and combine the two components into a single scalar reward through weighted summation. Correspondingly, $r(t)$ is defined as follows:

$$r(t) = -\rho_1 E_{total}(t) + \rho_2 F_{energy} - \bar{R} + \rho_3 R_w + R_{char}, \quad (22)$$

where ρ_1 and ρ_2 are normalization parameters to ensure equivalent order of magnitude between the first and second terms, which correspond to the two distinct optimization objectives in Eq. (19a). Furthermore, we guide the UAV's action by designing a three-component reward function, which includes an out-of-bound penalty (\bar{R}), terminal bias reward ($\rho_3 R_w$), and charging reward (R_{char}). These components are defined as follows.

- 1) *The out-of-bound penalty* \bar{R} is a positive constant that exceeds the typical reward magnitude within a single time slot, specifically designed to constrain movement within the permissible flight area.
- 2) *The terminal bias reward* $\rho_3 R_w$ provides differential rewards for accessing terminals based on their spatial distribution, where $\rho_3 \in [0, 1]$ modulates the impact of

this term, and R_w is formulated as:

$$R_w = R_b \sum_{i=1}^I w_i, \quad (23)$$

where R_b denotes the baseline reward parameter, and $w_i \in [0, 1]$ represents the accessibility challenge weight assigned to terminal i . Note that a terminal with greater accessibility challenges means that it is more difficult for the UAV to explore the terminal and therefore will have a larger weight w_i , thereby incentivizing the UAV to explore trajectories that incorporate these difficult-to-reach terminals.

- 3) *The charging reward R_{char}* primarily incentivizes the UAV to prioritize terminals with lower energy levels, thus promoting efficient resource allocation, defined as follows:

$$R_{char} = \begin{cases} 0 & \text{if no communication,} \\ \Delta E_{charging}(t) + C & \text{if communicating with} \\ & \text{the lowest-energy terminal,} \\ \Delta E_{charging}(t) & \text{otherwise.} \end{cases} \quad (24)$$

where $\Delta E_{charging}(t)$ denotes the energy increase of the target terminal during time slot t , and C is a positive constant that provides additional reward for charging the lowest-energy terminal.

After establishing this MDP framework, we subsequently introduce the standard SAC algorithm.

C. SAC Algorithm

SAC is an off-policy actor-critic DRL algorithm based on the maximum entropy RL framework. Unlike on-policy methods, off-policy methods typically utilize experience replay buffers to enhance sampling efficiency, making it appropriate for our MDP with large variations in transitions. Compared to other common off-policy methods, the maximum entropy framework enables SAC to effectively handle high-dimensional, complex continuous action spaces while providing superior convergence and stability [49].

Unlike other DRL methods, SAC incorporates two objectives: maximizing cumulative rewards and maintaining policy stochasticity. Specifically, the core innovation of this algorithm is the inclusion of an entropy regularization term in the objective function, enabling the agent to preserve exploration capability during convergence [50]. The optimal policy objective with entropy can be formalized as follows:

$$\pi^* = \arg \max_{\pi} \sum_t \mathbb{E}_{(s_t, a_t) \sim \rho_{\pi}} [r(s_t, a_t) + \alpha \mathcal{H}(\pi(\cdot|s_t))], \quad (25)$$

where $\mathcal{H}(\pi(\cdot|s_t))$ represents the policy entropy under state s_t , quantifying the randomness in action selection. The temperature parameter α functions as a regularization coefficient that balances entropy maximization against reward optimization, significantly affecting convergence performance. Moreover, the authors in [51] propose an automatic adjustment method for α , with the corresponding loss function as follows:

$$L(\alpha) = \mathbb{E}_{a_t \sim \pi_t} [-\alpha \log \pi_t(a_t|s_t) - \alpha \bar{\mathcal{H}}]. \quad (26)$$

However, the standard SAC algorithm faces several limitations in practical applications. First, its convergence stability

is problematic. Standard SAC typically employs multi-layer perceptrons (MLPs) as function approximators [52], [53], but these networks often exhibit unstable convergence and overfitting when handling MDPs with numerous parameters [54]. Second, the hybrid action space in our MDP, which combines discrete and continuous actions, presents inherent difficulties for standard SAC implementation. Third, significant variability in immediate rewards impedes effective policy evaluation by neural networks. Based on these challenges, we aim to enhance the standard SAC algorithm to achieve faster and more stable convergence in complex dynamic environments.

D. SAC-SK Framework

In this part, we propose the SAC-SK algorithm, which integrates three enhancement modules: the action simplification mechanism, simple recurrent unit (SRU), and modified Kolmogorov-Arnold networks (KAN). SAC-SK optimizes the flight trajectories of the UAV through the optimization of a normalized scalar reward function, thereby addressing the formulated problem. We first detail each module individually, then examine the comprehensive architecture and operational principles of the SAC-SK framework.

1) *Action Simplification Mechanism*: The standard SAC algorithm exhibits poor convergence and performance limitations when dealing with hybrid action spaces in our MDP framework. To address this issue, we propose an action simplification mechanism based on a greedy strategy. Specifically, through theoretical analysis of system operations, we develop a dynamic decision-making approach to replace original discrete decision variables, effectively transforming the hybrid action space into a continuous one.

To simplify the action space, we analyze the energy components $E_{i \rightarrow u}(t)$, $E_{u \rightarrow i}(t)$, and $E_{u \rightarrow tran}(t)$ within a single time slot, as these variables directly correlate with the UAV-terminal distance. In contrast, $E_{u \rightarrow move}(t)$ depends on both flight time and velocity [17]. With a constant volume of offloadable task data and communication distance d_{u-i} , the relationship between energy consumption and d_{u-i} can be analyzed as follows:

- 1) According to the first part of the Eq. (13), $E_{i \rightarrow tran}(t)$ is proportional to the offloading time τ_{up} , where $\tau_{up} \propto \frac{1}{R_{i \rightarrow u}}$. From Eqs. (2), (3), and (6), we establish that $R_{i \rightarrow u} \propto h_i^t G_i^t \propto \frac{1}{d_{u-i}}$. Thus, $E_{i \rightarrow tran}(t) \propto d_{u-i}$.
- 2) According to the second part of the Eq. (12), SWIPT divides $E_{u \rightarrow tran}(t)$ into energy transmission and information transmission components. The total transmission time is determined by $\max\left(\frac{1}{R_{u \rightarrow i}}, \frac{1}{E_{u \rightarrow i}(t)}\right)$, making $E_{u \rightarrow tran}(t)$ proportional to this value. Based on Eqs. (4), (5), and (8), both $R_{u \rightarrow i}$ and $E_{u \rightarrow i}(t)$ are proportional to G_i^t . Consequently, $E_{u \rightarrow tran}(t) \propto d_{u-i}$ and $E_{u \rightarrow i}(t) \propto \frac{1}{d_{u-i}}$.

Our analysis reveals that as the UAV approaches the terminal, both $E_{i \rightarrow tran}(t)$ and $E_{u \rightarrow tran}(t)$ decrease proportionally, while $E_{u \rightarrow i}(t)$ exhibits a significant increase. Additionally, $E_{u \rightarrow move}(t)$ reaches its minimum value when the UAV maintains a constant flight velocity of 10 m/s [55].

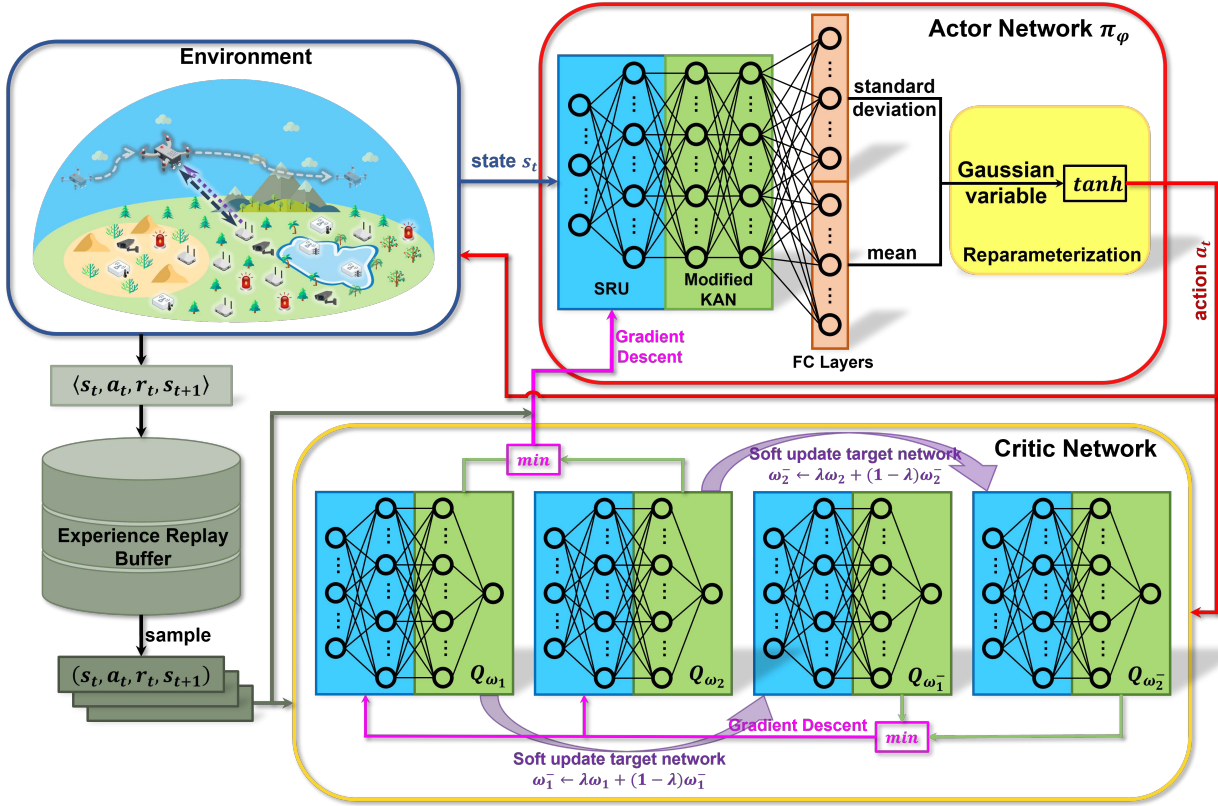


Fig. 3. The architecture of SAC-SK, where the SRU layer and the modified KAN layer are integrated into the neural networks.

Therefore, under ideal conditions, maintaining a flight velocity of 10 m/s and communicating with the closest terminal minimizes $\sum_{t=1}^T E_{total}(t)$. However, this policy fails to guarantee maximization of $\sum_{t=1}^T F_{energy}(t)$, potentially creating energy replenishment imbalances among terminals. Consequently, the UAV needs to dynamically explore optimal flight velocities v^t and angles θ^t . Regarding offloading decisions, we simplify the process by directing communication exclusively to the nearest terminal with offloadable tasks, thereby reducing model complexity. The action space is thus restructured as follows:

$$a_t = \{v^t, \theta^t\}, t \in \mathcal{T}. \quad (27)$$

This dimensional reduction to a two-dimensional continuous action space substantially improves learning efficiency.

2) *SRU*: Our MDP encompasses a large state space that incorporates environmental information and long-term dependencies, posing challenges for standard SAC algorithms to converge accurately and rapidly. To overcome this limitation, we introduce the SRU [56] for sequence modeling. SRU functions as a lightweight recurrent unit that delivers enhanced computational efficiency, improved scalability, and robust mathematical modeling while enabling high parallelization. In particular, the architectural framework of a single-layer SRU comprises two essential functional modules, which are a lightweight recurrence and a highway network.

Compared to conventional recurrent architectures such as long short-term memory (LSTM) [57] and gated recurrent units (GRU) [58], SRU strikes a balance between sequence dependence and independence. This design circumvents com-

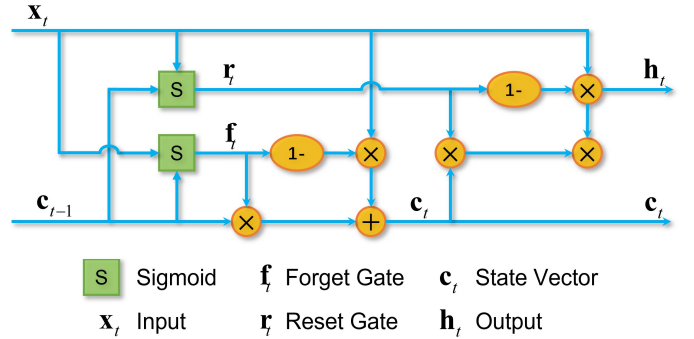


Fig. 4. The schematic of SRU calculative architecture.

putational bottlenecks associated with temporal dependencies while enabling parallel computation, significantly enhancing processing speed and GPU resource utilization. As illustrated in Fig. 4, SRU implements a forget gate f_t to regulate information flow, where the current state vector c_t is computed by integrating f_t with the previous state c_{t-1} and current input x_t . Through this mechanism, SRU effectively preserves long-term dependencies in sequential data.

The integration of SRU yields a computational framework characterized by both structural elegance and representational power, while simultaneously offering exceptional scaling properties through enhanced parallel processing capabilities and optimized gradient transmission pathways. Moreover, SRU efficiently captures temporal dependencies and contextual information while significantly reducing computational complexity.

3) *Modified KAN*: MLPs frequently struggle to effectively capture and extract latent information from complex sequential

data, resulting in performance bottlenecks during challenging training scenarios. To overcome these limitations, we introduce the KAN [59], a promising neural architecture derived from the Kolmogorov-Arnold representation theorem that significantly enhances mathematical fitting accuracy. The architectural distinctiveness of the KAN framework manifests in its fundamental reformulation of inter-neuronal connections. Traditional fixed-coefficient parameters are replaced by dynamically learnable functions. Specifically, each traditional weight parameter at network intersections transitions to an adaptive univariate B-spline representation with comprehensive parameterization capabilities. Concurrently, computational nodes within this architecture implement straightforward signal aggregation without introducing additional transformation operations typically employed in traditional networks. This computational reorganization eliminates the rigid connectivity constraints characteristic of conventional neural architectures, instead enabling each pathway between processing units to exhibit autonomous adaptability. The resulting architecture demonstrates substantially enhanced capacity for nuanced information transmission control, thereby facilitating more sophisticated representational capabilities. Formally, a general L -layer KAN architecture can be expressed as:

$$\text{KAN}(\mathbf{x}) = \sum_{i_{L-1}=1}^{n_{L-1}} \phi_{L-1, i_L, i_{L-1}} \left(\cdots \left(\sum_{i_1=1}^{n_1} \phi_{1, i_2, i_1} \left(\sum_{i_0=1}^{n_0} \phi_{0, i_1, i_0}(x_{i_0}) \right) \right) \right), \quad (28)$$

where $\phi_{l,j,i}$ represents the activation function connecting the i th neuron in layer l to the j th neuron in layer $l+1$. These activation functions are constructed through a linear combination of basis functions $b(x)$ and spline functions, expressed as follows:

$$\phi(x) = w_b b(x) + w_s \text{spline}(x), \quad (29)$$

where $b(x) = x/(1+e^{-x})$ and $\text{spline}(x) = \sum_i c_i B_i(x)$, with w_b , w_s , and c_i serving as trainable parameters.

Note that the original KAN architecture demands substantial computational resources and employs complex network structures, thereby leading to prohibitive time complexity [59]. To mitigate these issues, we propose a streamlined KAN variant that reduces hidden layer dimensionality and prunes redundant network layers, thereby achieving significantly lower computational overhead. Despite architectural simplifications, our modified KAN framework maintains superior mathematical fitting capabilities, primarily due to the integration of SRU components and the inherent advantages of the KAN paradigm.

4) *SAC-SK Architecture*: In this part, we introduce the main architecture and procedures of SAC-SK.

Nevertheless, certain distinctions exist between the actor network and the critic networks.

As illustrated in Fig. 3, similar to conventional actor-critic frameworks, SAC-SK utilizes five enhanced neural networks, each integrating SRU layers and modified KAN layers. Specifically, the architecture processes input data (state s_t or transition batches) through SRU layers that extract environmental

Algorithm 1: SAC-SK Algorithm

Input: The locations $\{p_i\}_{i \in \mathcal{I}}$ of terminals and the location p_u^0 of the UAV.

Output: The velocity \mathcal{V} and angle ϑ of the UAV in every time slot.

- 1 Initialize parameters of actor network φ and soft Q networks ω_1, ω_2 randomly;
 - 2 Initialize parameters of target Q networks: $\omega_1^- \leftarrow \omega_1, \omega_2^- \leftarrow \omega_2$;
 - 3 Initialize experience replay buffer $\mathcal{B} = \emptyset$;
 - 4 **for** iteration $m = 1$ to M **do**
 - 5 **if** Meet reset condition **then**
 - 6 Reset environment with same random seed;
 - 7 **for** time slot $t = 1$ to T **do**
 - 8 Select action $a_t \sim \pi_\varphi(s_t)$;
 - 9 Get velocity $v_m(t)$ and angle $\theta_m(t)$ from a_t ;
 - 10 Execute action a_t ;
 - 11 Observe reward r_t and next state s_{t+1} ;
 - 12 $\mathcal{B} \leftarrow \langle s_t, a_t, r_t, s_{t+1} \rangle$;
 - 13 **if** Reach batch threshold **then**
 - 14 Sample transitions $\{ \langle s_b, a_b, r_b, s_{b+1} \rangle \}_{b=1, \dots, B_s}$ from \mathcal{B} ;
 - 15 Update soft Q network according to [51];
 - 16 Reparameterize and resample the new action;
 - 17 Update actor network according to [51];
 - 18 Update temperature parameter α according to Eq. (26);
 - 19 Soft update target Q network $\omega_i^- \leftarrow \lambda \omega_i + (1 - \lambda) \omega_i^-, i = 1, 2$;
 - 20 $\mathcal{V} \leftarrow v_m(t)$;
 - 21 $\vartheta \leftarrow \theta_m(t)$;
 - 22 **return** \mathcal{V}, ϑ .
-

information, maintain long-term dependencies, and generate a hidden information vector. This vector is subsequently processed by modified KAN layers, which leverage their mathematical representation capabilities for fitting. Nevertheless, the actor and critic networks differ in their output structures:

- *Actor Network*: As shown in Fig. 5(a), two parallel fully connected layers (FC layers) process the modified KAN output to generate the mean and standard deviation of the action distribution, respectively.
- *Critic Networks*: As shown in Fig. 5(b), the modified KAN layers directly output a scalar value.

Algorithm 1 outlines the main steps of the SAC-SK algorithm. The procedure begins with network parameter initialization, followed by environment reset using consistent random seeds to ensure standardized initial conditions across episodes. During each time slot t , the algorithm: (1) selects action a_t based on the current policy. (2) Executes the action to obtain transition $\langle s_t, a_t, r_t, s_{t+1} \rangle$. (3) Stores the transition in experience replay buffer \mathcal{B} . Once \mathcal{B} reaches the predetermined threshold, SAC-SK samples transition batches for training and updates all neural networks along with the temperature parameter α . This process iterates until reaching the preset time step limit, progressively approximating an optimal maximum

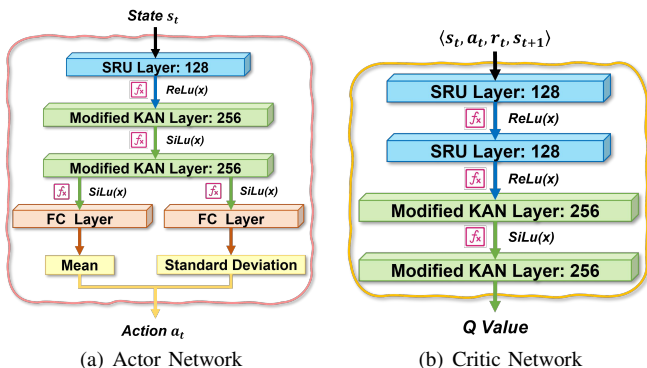


Fig. 5. The neural network architecture of SAC-SK.

entropy policy.

5) *Complexity Analyses*: In this part, we analyze the computational and space complexity of the proposed SAC-SK algorithm in both the training phase and the execution phase.

Training Phase: The computational complexity of SAC-SK [60] is $\mathcal{O}(|\varphi| + 4|\Omega| + MTK + MT|\varphi| + MT(2|\Omega|) + MT/(4|\Omega|))$ in the training phase, which can be summarized as follows:

- **Network Initialize**: This phase involves the initialization of the neural network parameters. Specifically, the computational complexity is expressed as $\mathcal{O}(|\varphi| + 4|\Omega|)$, where $|\varphi|$ denotes the number of parameters in the actor network, and $|\Omega|$ represents the average number of parameters in the four critic networks, which are $|\omega_1|$, $|\omega_2|$, $|\omega_1^-|$, and $|\omega_2^-|$, respectively, since these parameters are of the same order of magnitude.
- **Replay Buffer Collection**: The complexity of collecting state transitions in the experience replay buffer is $\mathcal{O}(MTK)$, where M is the number of training episodes, T denotes the number of steps in an episode (i.e., the total number of time slots in the scenario), and K represents the complexity of interacting with the environment.
- **Network Update**: The updating phase is divided into three main parts, which are the updates of the actor network, the frequent updates of the soft Q networks, and the respective soft updates of target Q networks, respectively. Note that the temperature parameter α is a single parameter, so its update complexity is negligible. Therefore, the complexity for this phase is calculated as $\mathcal{O}(MT|\varphi| + MT(2|\Omega|) + MT/(4|\Omega|))$.

The space complexity of SAC-SK accounts for the storage of the neural network parameters and the transition structures $\langle s_t, a_t, r_t, s_{t+1} \rangle$ required to maintain the experience replay buffer \mathcal{B} . Therefore, the space complexity can be calculated as $\mathcal{O}(|\varphi| + 4|\Omega| + |\mathcal{B}|(2|s| + |a| + 1))$, where $|\mathcal{B}|$ represents the size of \mathcal{B} , while $|s|$ and $|a|$ represent the dimensions of the state space and action space, respectively.

Execution Phase: First, the computational complexity of SAC-SK is $\mathcal{O}(MT|\varphi|)$, resulting from the action selection based on the current state using the actor network. Second, the space complexity of SAC-SK is $\mathcal{O}(|\varphi|)$, primarily stemming from the parameters of the actor network.

E. Practical Implementation of SAC-SK-based UAV Management

In this part, we elaborate on the application methodology of the proposed solution in practical scenarios, specifically divided into the training and deployment phase [48].

1) *Training Phase*: During the training phase, the neural network is initially trained in a simulation environment before deployment. Specifically, the proposed SAC-SK method does not depend on pre-collected real-world data. Instead, it interacts with a simulation environment constructed using mathematical models. Through this interaction, the SAC-SK algorithm gathers data to train the policy. We emphasize that our simulation is realistic, incorporating state-of-the-art mathematical models, including the air-to-ground channel model, non-linear EH model, energy consumption models for the UAV and terminals, and task computation models, among others. These models are derived from or based on real-world data, thereby ensuring the simulation environment closely reflects actual conditions. Consequently, the policy trained in this simulation can be effectively applied to real-world scenarios.

2) *Deployment Phase*: During the deployment phase, the pre-trained SAC-SK algorithm dynamically interacts with physical environments by processing real-time state data for decision generation. The SAC-SK strategies can be effectively implemented through the central control unit. Given that the UAV and terminals incorporate geolocation capabilities, the central control unit seamlessly obtains positional coordinates. During this phase, the SAC-SK eliminates the need for instantaneous calculations of transmission rates or energy expenditure metrics to determine reward values. Leveraging its acquired policy network, the system directly produces control commands that reflect predefined optimization objectives through existing spatial data (including device/UAV coordinates). The associated communication latency proves negligible since positional data transmission requires minimal bandwidth consumption.

3) *Environment Changes*: When encountering environmental variations, pre-trained neural networks demonstrate adaptive potential through iterative parameter recalibration in modified environments. Specifically, operators may adjust critical simulation parameters (including UAV transmit power, terminal location distribution, etc.) to facilitate DRL model re-optimization. Advanced methodologies like transfer learning [61] significantly accelerate retraining convergence, while integrated architectural enhancements, particularly the action simplification mechanism, SRU layers, and modified KAN layers, collectively optimize learning efficiency. Building upon these foundations, the synergistic integration of edge computing with incremental learning paradigms enables seamless real-time updates for field-deployed network systems.

V. SIMULATION AND ANALYSES

In this section, we evaluate the performance of the proposed SAC-SK algorithm for solving the formulated optimization problem, with specific emphasis on convergence properties and computational efficiency.

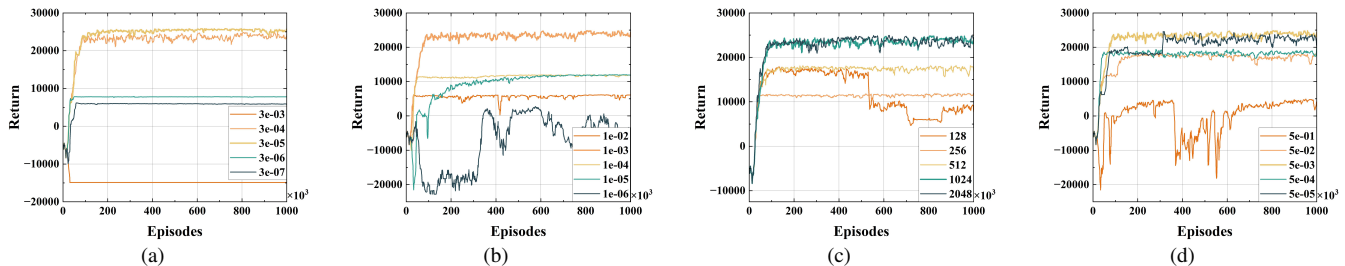


Fig. 6. Return under different key hyperparameters of SAC-SK. (a) The learning rate of the actor network λ_ϕ . (b) The learning rate of the critic network λ_ω . (c) The batch size of the sample B_s . (d) target smoothing coefficient λ .

A. Simulation Setups

In this part, we present the experimental setup, including scenario configuration, system parameters, baseline algorithms, and performance metrics.

1) *Simulation Setups*: In this work, we consider a scenario in which a UAV delivers both MEC and charging services to IoT terminals in a remote area. Specifically, the UAV operates at a fixed altitude of 10 m on a horizontal plane, with an initial position at the origin $(0, 0)$ in Cartesian coordinates and a maximum velocity of 30 m/s. The service operation spans 30 seconds, discretized into 30 equal time slots.

Moreover, we consider a 40×40 m² area without ground base stations, bounded by coordinates $\{(x, y) \mid x \in [-20, 20], y \in [-20, 20]\}$. Five IoT terminals are randomly distributed within this region using Poisson disk sampling to create a network topology centered around the origin. The defined boundary dimensions of 40 m provide sufficient space for UAV maneuverability during algorithm training. For larger geographical areas or more complex networks, clustering techniques such as k-means could partition the environment into multiple sub-regions, facilitating the deployment of multiple UAVs to execute our proposed method in each sub-network separately. Table I provides all relevant simulation parameters.

For the proposed SAC-SK algorithm, the network architecture is illustrated in Fig. 5, with parameters optimized through extensive experimentation. Specifically, the actor network comprises a single-layer SRU with a hidden dimension of 128, coupled with the modified KAN layers and FC layers, each containing two layers with 256 neurons. The critic networks implement two-layer structures for both the SRU and modified KAN, each with 128 neurons. These architectural choices result from systematic parameter optimization to maximize performance and ensure convergence stability.

2) *Baselines Algorithms*: Performance evaluation of the proposed SAC-SK algorithm involves comparative analysis against several advanced DRL algorithms, including SAC, deep deterministic policy gradient (DDPG), twin delayed deep deterministic policy gradient (TD3), and proximal policy optimization (PPO). Specifically:

- **SAC** [51]: The original SAC algorithm utilizes MLP-based neural networks, which are the basis for improvements of SAC-SK. Similar to IV-D5, the computational complexity of SAC is $\mathcal{O}(|\varphi| + 4|\Omega| + MTK + MT|\varphi| + MT(2|\Omega|) + MT/(4|\Omega|))$.

- **DDPG** [67]: A classic off-policy algorithm designed specifically for continuous action space environments, known for its deterministic policy gradients. Similar to IV-D5, the computational complexity of DDPG is $\mathcal{O}(2|\varphi| + 2|\Omega| + MTK + 2MT(|\varphi| + |\Omega|))$.
- **TD3** [68]: An enhanced variant of DDPG that addresses function approximation errors through twin delayed updates. Similar to IV-D5, the computational complexity of TD3 is $\mathcal{O}(2|\varphi| + 4|\Omega| + MTK + \frac{3}{2}MT|\varphi| + 4MT|\Omega|)$.
- **PPO** [69]: A robust on-policy method that employs actor-critic architecture while maintaining computational efficiency. Similar to IV-D5, the computational complexity of PPO is $\mathcal{O}(|\varphi| + |\Omega| + MTK + ME(|\varphi| + |\Omega|))$.

As can be seen, the computational complexity of the proposed SAC-SK is comparable to that of SAC, DDPG, TD3, and PPO. These methods share similar network architectures and training processes in deep reinforcement learning, thereby resulting in similar computational requirements.

B. Performance Evaluation

In this part, we present a systematic performance evaluation of the proposed SAC-SK and analyze its operational characteristics.

1) *Convergence Evaluations*: To investigate the convergence and stability of SAC-SK, we conduct a comprehensive analysis involving the following key algorithmic parameters:

- 1) *Discount factor γ* . The experimental framework utilizes a time step of 30 slots in an iteration, thereby necessitating the consideration of rewards extending to at least the 30th future step. Applying the formulation $\gamma \approx 0.1^{1/t}$ [70] with $t = 30$ yields a discount factor value of 0.92 approximately.
- 2) *Learning rate of actor network λ_ϕ* . Fig. 6(a) illustrates the impact of varying λ_ϕ values on convergence behavior. The results reveal that $\lambda_\phi = 3 \times 10^{-5}$ yields optimal convergence performance, demonstrating improvements over alternative values.
- 3) *Learning rate of critic networks λ_ω* . Fig. 6(b) demonstrates that both excessively small and large λ_ω values adversely affect convergence. Although $\lambda_\omega = 1 \times 10^{-4}$ facilitates rapid initial convergence, $\lambda_\omega = 1 \times 10^{-3}$ exhibits superior long-term convergence performance. Therefore, we set $\lambda_\omega = 1 \times 10^{-3}$ for optimal results.
- 4) *The batch size of sample B_s* . Fig. 6(c) illustrates that while batch size exhibits minimal influence on conver-

TABLE I
KEY SIMULATION SETTINGS

Symbol	Parameters	Values
f_c	Carrier frequency	2.4 GHz [4]
c	The speed of light	3×10^8 m/s [62]
$(\eta_{\text{LoS}}, \eta_{\text{NLoS}})$	Additional losses of LoS and NLoS links	(0.1, 21) [37]
(a_1, b_1)	Parameters of LoS probability	(4.88, 0.43) [37]
σ^2	Power of Gaussian white noise	-174 dBm/Hz [63]
P_{tran}	Transmit power of the UAV	40 W [8]
P_i	Transmit power of the terminals	100 mW [64]
B	Total bandwidth	1 MHz [55]
(a_2, b_2)	EH circuit parameters	(150, 0.014) [65]
P_{max}	The maximum received power of EH circuit	24 mW [65]
η	Power splitting ratio	0.8 [4], [8]
(k, ν)	Effective capacitance coefficient	$(10^{-28}, 3)$ [40]
ΔE_1	Daily energy consumption for terminals	$50 \mu\text{W}$ [42]
E_{max}	The maximum energy of terminal battery	$5 \mu\text{J}$
E_{min}	The minimum energy of terminal battery	$800 \mu\text{J}$
R_{min}	The minimum threshold of transmission rate	22 Mbps
$D_{i,p}^t$	Data size of the tasks	10^3 bit [64]
C_i	The task computation density	100 cycles/bit [4], [19]
f_u	The CPU frequency of the UAV	5 GHz [62]
f_i	The CPU frequency of the terminals	1 GHz [62]
v_{max}	The maximum velocity of the UAV	30 m/s [4]
I	Number of the terminals	5
H	Altitude of the UAV	5 m [4]
T	Number of time slots	30
τ	Length of one slot	1 s [8], [66]
-	The edge length of the area boundary	40 m
(ρ_1, ρ_2)	Normalization parameters	(0.3, 1)
C	The charging reward constant	300
\bar{R}	The out-of-bound penalty	800
R_b	The baseline of terminal bias reward	50
α	Initial temperature parameter	0.2
γ	Discount factor	0.92
λ_φ	Learning rate of actor network	3×10^{-4}
λ_ω	Learning rate of critic networks	10^{-3}
B_s	The batch size of sample	1024
λ	Target smoothing coefficient	5×10^{-3}
-	Size of experience replay buffer	10^6
-	Policy frequency	2
-	Target network frequency	1

gence relative to other hyperparameters (with the exception of $B_s = 128$), it substantially affects training stability. A batch size of $B_s = 1024$ was selected to optimize convergence stability throughout the training process.

- 5) *Target smoothing coefficient* λ . Fig. 6(d) demonstrates the influence of λ on convergence. The result shows that SAC-SK achieves optimal convergence at $\lambda = 5 \times 10^{-3}$, a parameter that controls the soft update mechanism for target Q networks as expressed by $\omega_i^- \leftarrow \lambda \omega_i + (1 - \lambda) \omega_i^-, i = 1, 2$.

In conclusion, we have identified the critical hyperparam-

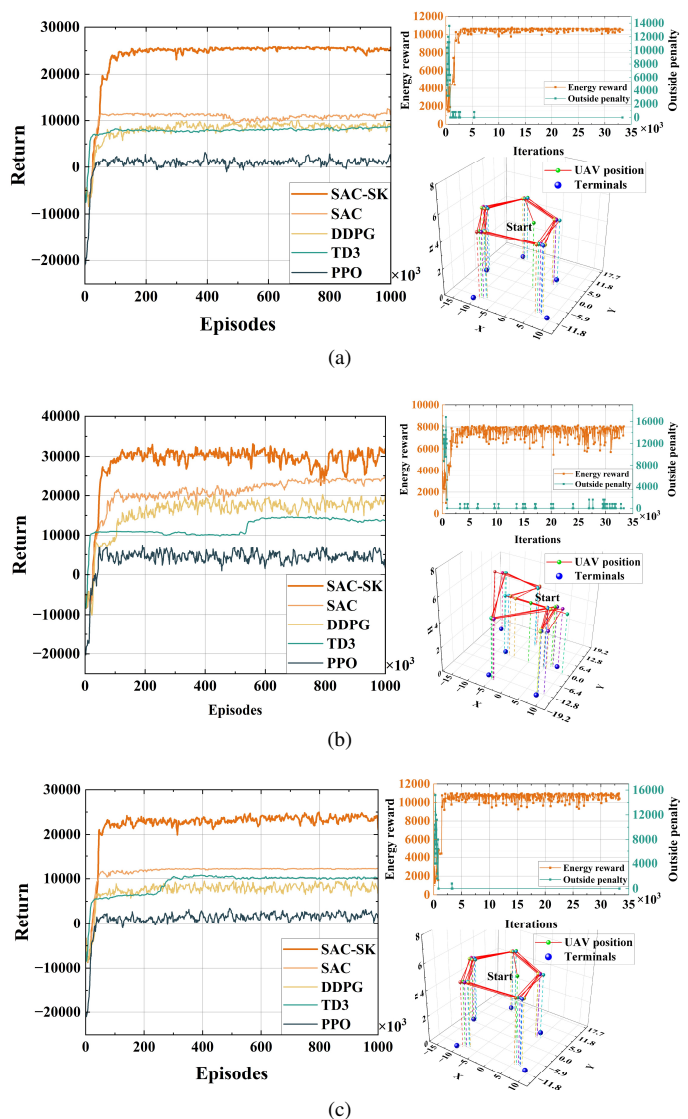


Fig. 7. Simulation results under different random seeds, in which each subfigure includes a comparison between SAC-SK and baselines, the variation of the out-of-bound penalty \bar{R} and the charging reward R_{char} with iterations, and the trajectory of the UAV. (a) seed=1. (b) seed=3. (c) seed=5.

ters of SAC-SK and demonstrated its convergence and stability through rigorous experimental evaluation. Table I summarizes the optimized hyperparameters derived from our systematic analysis.

2) *Comparisons with Different Baselines*: In this part, we conduct some simulations of SAC-SK to assess its robustness and effectiveness and evaluate its performance through comprehensive comparisons with various baselines.

To verify the generalization capability of the proposed SAC-SK, we conduct a series of comparative simulations under distinct spatial distributions of terminals within the simulation area. Specifically, we consider three representative simulation scenarios by using different random seeds [60]. These scenarios are shown in Figs. 7(a), 7(b) and 7(c), and the details are as follows:

- 1) The first case is uniform distribution. This scenario generates a relatively uniform spatial distribution of terminals, establishing a basic case for evaluating algorithm performance under standard conditions (Random seed=1 in this

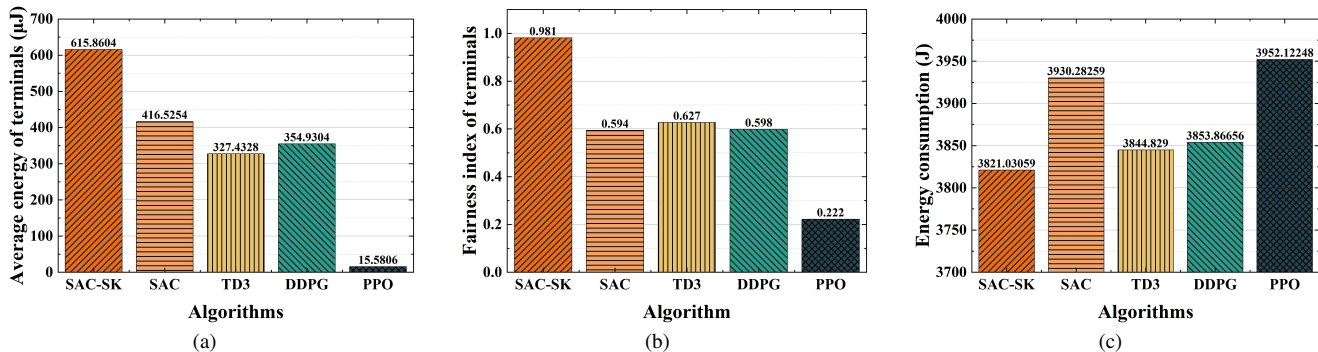


Fig. 8. Comparison results of SAC-SK and DRL-based algorithms. (a) Average retained energy of terminals. (b) Charging fairness among terminals. (c) Total energy consumption of the system.

case).

- 2) The second case is a clustered distribution. This scenario features a high-density cluster of terminals with one outlier positioned at a significant distance from the main group. This configuration evaluates the convergence behavior of the algorithms to optimize trajectories when faced with potential local optima and coverage trade-offs (Random seed=3 in this case).
- 3) The third case is asymmetric distribution. This scenario presents a terminal arrangement in which the terminal distribution center is significantly offset from the initial position of the UAV. This configuration evaluates the algorithms' exploration capabilities and adaptability to spatially biased configurations (Random seed=5 in this case).

As illustrated in Fig. 7, the proposed SAC-SK consistently outperforms all baselines across diverse random seeds, demonstrating robust generalization capability and efficient environmental information utilization.

In Fig. 8, we present three key performance metrics for the optimization objectives and compare SAC-SK against multiple baselines. These metrics are the average retained energy of terminals, charging fairness among terminals, and system energy consumption, respectively. As evidenced in Figs. 8(a) and 8(b), SAC-SK demonstrates substantial performance advantages over all baselines. Specifically, SAC-SK achieves 47.86% higher average retained energy and 65.15% improved charging fairness compared to standard SAC. These results confirm the effectiveness of SAC-SK in simultaneously maximizing terminal battery energy while ensuring fair charging distribution across all terminals. Furthermore, Fig. 8(c) reveals that SAC-SK achieves the lowest system energy consumption among all tested algorithms, reducing consumption by 109.252 J relative to SAC. While TD3 and DDPG also exhibit lower energy consumption than SAC, the apparent efficiency of TD3 and DDPG is attributable to their suboptimal exploration patterns. The performance of TD3 and DDPG in inferior fairness indices (0.627 and 0.598, respectively) and average terminal energy levels (327.4328 μJ and 354.9304 μJ , respectively) indicates convergence to local optima due to incomplete terminal coverage. In conclusion, SAC-SK successfully balances the inherent trade-off between the bi-objective optimization and

delivering superior performance across all evaluation metrics.

Moreover, we conduct comprehensive performance analyses across all algorithms. The key findings are as follows:

- 1) First, as an on-policy algorithm, PPO consistently underperforms compared to the off-policy algorithms across all random seeds. This performance gap is attributable to the experience replay mechanism in off-policy algorithms, which facilitates more efficient utilization of high-value transitions, thereby enhancing performance in complex environments.
- 2) Second, SAC demonstrates superior convergence performance relative to DDPG and TD3, as evidenced by Figs. 7(a), 7(b), and 7(c). This result indicates that SAC provides a more effective foundation for algorithmic enhancement than other popular DRL algorithms. Specifically, the performance advantage derives from the maximum entropy RL framework, which simultaneously optimizes cumulative rewards and action randomness, thus improving both exploration efficiency and algorithmic robustness.
- 3) Third, SAC-SK achieves superior convergence through its integration of SRU preprocessing for state-action inputs and modified KAN fitting for hidden information, thereby achieving the effectiveness of its action selection strategy. Comparative analysis across different random seeds confirms this finding. As illustrated in Fig. 7(b), even in the most challenging scenario with complex terminal distribution (seed = 3), SAC-SK maintains a performance advantage with average return approximately 4000 values higher than SAC. This performance differential increases to over 10000 values in other scenarios, as evidenced by Figs. 7(a) and 7(c). Simulation results demonstrate that integrating SRU as a temporal encoder effectively addresses the limitation of standard SAC in capturing temporal correlations in partially observable environments, while achieving preliminary modeling of environmental information and long-term dependencies with higher computational efficiency. Meanwhile, incorporating KAN as a function approximator effectively mitigates the deficiency of MLPs in standard SAC, where fixed activation patterns exhibit insufficient mathematical approximation capability for complex hidden information.

Furthermore, we conduct a detailed analysis of the charging reward R_{char} and the out-of-bound penalty \bar{R} . As shown in the upper right corners of Figs. 7(a), 7(b), and 7(c), the training process exhibits three distinct phases. In the initial phase (iterations 0 - 2000 approximately), the UAV learns boundary constraints, evidenced by \bar{R} decreasing to zero. Correspondingly, random exploration of the UAV yields communication links with terminals, thereby causing rapid increases in R_{char} . During the intermediate phase (iterations 2000 - 5000 approximately), the UAV systematically explores the valid operational area, acquires terminal distribution information, and develops long-term memory representations. Concurrently, the experience replay buffer reaches its training threshold. This phase demonstrates reduced R_{char} growth rate due to the increased complexity of reward maximization. The final phase (beyond 5000 iterations) achieves convergence stability while maintaining exploration of high-entropy strategies. These observations confirm that the designed reward function $r(t)$ effectively guides SAC-SK toward convergence.

Additionally, we visualize the flight trajectory of the UAV and its spatial relationships with ground terminals through a 3D format to present the results more intuitively.

VI. CONCLUSION

In this paper, we have investigated a directional antenna-enhanced UAV-assisted multi-terminal SWIPT-MEC system operating in infrastructure-free environments. Specifically, we have proposed a novel architecture wherein a UAV functions as both a base station and MEC server to provide charging and computational offloading services for energy-constrained ground terminals. In this system, we have formulated a bi-objective optimization problem to minimize system energy consumption and simultaneously maximize terminal battery energy while ensuring charging fairness among terminals. Subsequently, we have reformulated the original problem into an MDP to enhance computational tractability and system scalability. To address this MDP, we have proposed the SAC-SK algorithm to learn a maximum entropy optimal policy, thereby efficiently scheduling offloading decisions and UAV trajectory planning. Simulation results have demonstrated that SAC-SK significantly outperforms baselines across multiple performance metrics, while exhibiting robust generalization capabilities in diverse scenarios. This study has several limitations that are worth considering. First, static ground terminals may not fully capture the dynamics of real-world mobile scenarios. Second, the energy consumption model does not account for potential signal interference in dense deployment environments. Finally, although SAC-SK optimizes the time complexity and computational load during the training process, it still requires non-negligible computational resources, which may limit its practical deployment in resource-constrained UAV platforms. Future work will be extended along four dimensions, which include dynamic user mobility modeling, multi-UAV coordination, more lightweight neural network architectures, and the integration of digital twin technology and blockchain-based solutions.

REFERENCES

- [1] H. Pan, Y. Liu, G. Sun, J. Fan, S. Liang, and C. Yuen, "Joint power and 3D trajectory optimization for UAV-enabled wireless powered communication networks with obstacles," *IEEE Trans. Commun.*, vol. 71, no. 4, pp. 2364–2380, Jun. 2023.
- [2] T. Vu, T. Nguyen, and S. Kim, "Cooperative NOMA-enabled SWIPT IoT networks with imperfect SIC: performance analysis and deep learning evaluation," *IEEE Internet Things J.*, vol. 9, no. 3, pp. 2253–2266, Jun. 2022.
- [3] Z. Su, W. Feng, J. Tang, Z. Chen, Y. Fu, N. Zhao, and K. Wong, "Energy-efficiency optimization for D2D communications underlaying UAV-assisted industrial IoT networks with SWIPT," *IEEE Internet Things J.*, vol. 10, no. 3, pp. 1990–2002, Jan. 2023.
- [4] X. Zhou, L. Huang, T. Ye, and W. Sun, "Computation bits maximization in UAV-assisted MEC networks with fairness constraint," *IEEE Internet Things J.*, vol. 9, no. 21, pp. 20997–21009, May 2022.
- [5] Y. Li, H. Kang, J. Li, G. Sun, Z. Sun, J. Wang, C. Zhao, and D. Niyato, "A correlated data-driven collaborative beamforming approach for energy-efficient IoT data transmission," *IEEE Internet Things J.*, Feb. 2025, early access.
- [6] D. C. Nguyen, M. Ding, P. N. Pathirana, A. Seneviratne, J. Li, D. Niyato, O. A. Dobre, and H. V. Poor, "6G internet of things: A comprehensive survey," *IEEE Internet Things J.*, vol. 9, no. 1, pp. 359–383, Aug. 2022.
- [7] K. W. Choi, S. I. Hwang, A. A. Aziz, H. H. Jang, J. S. Kim, D. S. Kang, and D. I. Kim, "Simultaneous wireless information and power transfer (SWIPT) for internet of things: novel receiver design and experimental validation," *IEEE Internet Things J.*, vol. 7, no. 4, pp. 2996–3012, Jan. 2020.
- [8] R. Jiang, K. Xiong, H. Yang, P. Fan, Z. Zhong, and K. B. Letaief, "On the coverage of UAV-assisted SWIPT networks with nonlinear EH model," *IEEE Trans. Wirel. Commun.*, vol. 21, no. 6, pp. 4464–4481, Dec. 2022.
- [9] Y. Qu, H. Sun, C. Dong, J. Kang, H. Dai, Q. Wu, and S. Guo, "Elastic collaborative edge intelligence for UAV swarm: Architecture, challenges, and opportunities," *IEEE Commun. Mag.*, vol. 62, pp. 62–68, Jan. 2024.
- [10] X. Wang and M. C. Gursoy, "Coverage analysis for energy-harvesting UAV-assisted mmwave cellular networks," *IEEE J. Sel. Areas Commun.*, vol. 37, no. 12, pp. 2832–2850, Oct. 2019.
- [11] Z. Sun, G. Sun, L. He, F. Mei, S. Liang, and Y. Liu, "A two time-scale joint optimization approach for UAV-assisted MEC," in *Proc. IEEE INFOCOM*, Aug. 2024, pp. 91–100.
- [12] M. Yan, R. Xiong, Y. Wang, and C. Li, "Edge computing task offloading optimization for a UAV-assisted internet of vehicles via deep reinforcement learning," *IEEE Trans. Veh. Technol.*, vol. 73, pp. 5647–5658, Apr. 2024.
- [13] J. Wang, H. Du, G. Sun, J. Kang, H. Zhou, D. Niyato, and J. Chen, "Optimizing 6G integrated sensing and communications (ISAC) via expert networks," *arXiv preprint arXiv:2406.00408*, Jun. 2024.
- [14] J. Wang, H. Du, D. Niyato, J. Kang, S. Cui, X. Shen, and P. Zhang, "Generative AI for integrated sensing and communication: Insights from the physical layer perspective," *IEEE Wirel. Commun.*, vol. 31, no. 5, pp. 246–255, Jul. 2024.
- [15] J. Wang, C. Zhao, H. Du, G. Sun, J. Kang, S. Mao, D. Niyato, and D. I. Kim, "Generative AI enabled robust data augmentation for wireless sensing in ISAC networks," *arXiv preprint arXiv:2502.12622*, Feb. 2025.
- [16] W. Wang, X. Li, M. Zhang, K. Cumanan, D. W. K. Ng, G. Zhang, J. Tang, and O. A. Dobre, "Energy-constrained UAV-assisted secure communications with position optimization and cooperative jamming," *IEEE Trans. Commun.*, vol. 68, no. 7, pp. 4476–4489, Apr. 2020.
- [17] G. Sun, J. Li, Y. Liu, S. Liang, and H. Kang, "Time and energy minimization communications based on collaborative beamforming for UAV networks: A multi-objective optimization method," *IEEE J. Sel. Areas Commun.*, vol. 39, no. 11, pp. 3555–3572, Jun. 2021.
- [18] B. Wang, H. Kang, J. Li, G. Sun, Z. Sun, J. Wang, and D. Niyato, "UAV-assisted joint mobile edge computing and data collection via matching-enabled deep reinforcement learning," *IEEE Internet Things J.*, pp. 1–1, Feb. 2025, early access.
- [19] G. Sun, L. He, Z. Sun, Q. Wu, S. Liang, J. Li, D. Niyato, and V. C. M. Leung, "Joint task offloading and resource allocation in aerial-terrestrial UAV networks with edge and fog computing for post-disaster rescue," *IEEE Trans. Mob. Comput.*, vol. 23, no. 9, pp. 8582–8600, Jan. 2024.
- [20] G. Sun, J. Xiao, J. Li, J. Wang, J. Kang, D. Niyato, and S. Mao, "Aerial reliable collaborative communications for terrestrial mobile users via evolutionary multi-objective deep reinforcement learning," *IEEE Trans. Mob. Comput.*, vol. abs/2502.05824, Jan. 2025, early access.

- [21] Z. Sun, G. Sun, Q. Wu, L. He, S. Liang, H. Pan, D. Niyato, C. Yuen, and V. C. M. Leung, "TJCCCT: a two-timescale approach for UAV-assisted mobile edge computing," *IEEE Trans. Mob. Comput.*, vol. 24, no. 4, pp. 3130–3147, Mar. 2025.
- [22] D. E. Widiyanti and S. Y. Shin, "RIS-assisted MEC computation offloading for IoVT networks," in *Proc. IEEE ICTC*, Feb. 2023, pp. 214–217.
- [23] F. Song, H. Xing, X. Wang, S. Luo, P. Dai, Z. Xiao, and B. Zhao, "Evolutionary multi-objective reinforcement learning based trajectory control and task offloading in UAV-assisted mobile edge computing," *IEEE Trans. Mob. Comput.*, vol. 22, no. 12, pp. 7387–7405, Sep. 2023.
- [24] Y. Zeng, S. Chen, Y. Cui, J. Yang, and Y. Fu, "Joint resource allocation and trajectory optimization in UAV-enabled wirelessly powered MEC for large area," *IEEE Internet Things J.*, vol. 10, no. 17, pp. 15705–15722, Aug. 2023.
- [25] Y. Du, K. Yang, K. Wang, G. Zhang, Y. Zhao, and D. Chen, "Joint resources and workflow scheduling in UAV-enabled wirelessly-powered MEC for IoT systems," *IEEE Trans. Veh. Technol.*, vol. 68, no. 10, pp. 10187–10200, Aug. 2019.
- [26] Y. Liu, K. Xiong, Q. Ni, P. Fan, and K. B. Letaief, "UAV-assisted wireless powered cooperative mobile edge computing: Joint offloading, CPU control, and trajectory optimization," *IEEE Internet Things J.*, vol. 7, no. 4, pp. 2777–2790, Oct. 2020.
- [27] W. Liu, H. Wang, X. Zhang, H. Xing, J. Ren, Y. Shen, and S. Cui, "Joint trajectory design and resource allocation in UAV-enabled heterogeneous MEC systems," *IEEE Internet Things J.*, vol. 11, no. 19, pp. 30817–30832, Oct. 2024.
- [28] D. P. P. R. Baduge, T. D. P. Perera, and D. N. K. Jayakody, "Flight to efficiency: Trajectory optimization in SWIPT-enabled UAV-assisted NOMA for future wireless networks," in *Proc. IEEE VTC*, Dec. 2024, pp. 1–7.
- [29] K. Heo, H.-H. Choi, and K. Lee, "Joint trajectory and resource optimization for UAV-assisted SWIPT systems: A comparative study of linear and nonlinear energy harvesting models," *IEEE Internet Things J.*, vol. 11, no. 24, pp. 40293–40305, Sep. 2024.
- [30] J. Jalali, A. Khalili, H. Tabassum, R. Berkvens, J. Famaey, and W. Saad, "Energy-efficient THz NOMA for SWIPT-aided miniature UAV networks," *IEEE Commun. Lett.*, vol. 28, no. 5, pp. 1107–1111, May 2024.
- [31] W. Feng, J. Tang, Y. Yu, J. Song, N. Zhao, G. Chen, K. Wong, and J. A. Chambers, "UAV-enabled SWIPT in IoT networks for emergency communications," *IEEE Wirel. Commun.*, vol. 27, no. 5, pp. 140–147, Nov. 2020.
- [32] Z. Shi, X. Xie, H. Lu, H. Yang, Z. Xiong, J. Cai, and Z. Ding, "DRL-based multidimensional resource management in SWIPT-NOMA-enabled MEC," *IEEE Trans. Wirel. Commun.*, vol. 23, no. 4, pp. 3252–3266, May 2024.
- [33] K. Chhea, S. Mui, and J.-R. Lee, "Energy efficiency optimization in intelligent reflecting surface-aided UAV wireless power transfer networks using DRL," *IEEE Trans. Veh. Technol.*, pp. 1–11, Dec. 2024, early access.
- [34] R. Jiang, K. Xiong, H. Yang, J. Cao, Z. Zhong, and B. Ai, "Coverage performance of UAV-assisted SWIPT networks with directional antennas," *IEEE Internet Things J.*, vol. 9, no. 13, pp. 10600–10609, Aug. 2022.
- [35] Y. Meng, Z. Zhang, Y. Huang, and P. Zhang, "Queuing analysis of energy harvesting-aided NOMA-MEC network," *IEEE Trans. Veh. Technol.*, vol. 73, no. 9, pp. 14068–14073, Oct. 2024.
- [36] L. Wang, K. Wang, C. Pan, W. Xu, N. Aslam, and A. Nallanathan, "Deep reinforcement learning based dynamic trajectory control for UAV-assisted mobile edge computing," *IEEE Trans. Mob. Comput.*, vol. 21, no. 10, pp. 3536–3550, Sep. 2022.
- [37] R. I. B. Yaliniz, A. El-Keyi, and H. Yanikomeroglu, "Efficient 3-D placement of an aerial base station in next generation cellular networks," in *Proc. IEEE ICC*, Dec. 2016, pp. 1–5.
- [38] Y. Zeng, Q. Wu, and R. Zhang, "Accessing from the sky: A tutorial on UAV communications for 5G and beyond," *Proc. IEEE*, vol. 107, no. 12, pp. 2327–2375, May 2019.
- [39] E. Boshkovska, D. W. K. Ng, N. Zlatanov, and R. Schober, "Practical non-linear energy harvesting model and resource allocation for SWIPT systems," *IEEE Commun. Lett.*, vol. 19, no. 12, pp. 2082–2085, Sep. 2015.
- [40] F. Jiang, K. Wang, L. Dong, C. Pan, W. Xu, and K. Yang, "Deep-learning-based joint resource scheduling algorithms for hybrid MEC networks," *IEEE Internet Things J.*, vol. 7, no. 7, pp. 6252–6265, Jan. 2020.
- [41] Y. Zeng, J. Xu, and R. Zhang, "Energy minimization for wireless communication with rotary-wing UAV," *IEEE Trans. Wirel. Commun.*, vol. 18, no. 4, pp. 2329–2345, Sep. 2019.
- [42] L. Chai, L. Bai, T. Bai, J. Choi, and W. Zhang, "RIS-aided SCMA-based SWIPT systems: Design and optimization," *IEEE Trans. Veh. Technol.*, vol. 72, no. 5, pp. 6238–6252, Jun. 2023.
- [43] R. Jain, D. Chiu, and W. Hawe, "A quantitative measure of fairness and discrimination for resource allocation in shared computer systems," *arXiv preprint arXiv:9809099*, Jan. 1998.
- [44] G. Sun, B. Liu, J. Li, S. Liang, H. Pan, and X. Zheng, "Enabling urban mmwave communications with UAV-carried IRS via deep reinforcement learning," in *Proc. IEEE ICC*, Sep. 2024, pp. 4985–4990.
- [45] N. Zeng, Z. Wang, W. Liu, H. Zhang, K. Hone, and X. Liu, "A dynamic neighborhood-based switching particle swarm optimization algorithm," *IEEE Trans. Cybern.*, vol. 52, no. 9, pp. 9290–9301, Nov. 2022.
- [46] J. Li, G. Sun, Q. Wu, D. Niyato, J. Kang, A. Jamalipour, and V. C. M. Leung, "Collaborative ground-space communications via evolutionary multi-objective deep reinforcement learning," *IEEE J. Sel. Areas Commun.*, vol. 42, no. 12, pp. 3395–3411, Dec. 2024.
- [47] S. Liu, G. Sun, J. Li, S. Liang, Q. Wu, P. Wang, and D. Niyato, "UAV-enabled collaborative beamforming via multi-agent deep reinforcement learning," *IEEE Trans. Mob. Comput.*, vol. 23, no. 12, pp. 13015–13032, Nov. 2024.
- [48] G. Sun, J. Xiao, J. Li, J. Wang, J. Kang, D. Niyato, and S. Mao, "Aerial reliable collaborative communications for terrestrial mobile users via evolutionary multi-objective deep reinforcement learning," *IEEE Trans. Mob. Comput.*, vol. PP, pp. 1–18, Jan. 2025.
- [49] Y. Pu, S. Wang, R. Yang, X. Yao, and B. Li, "Decomposed soft actor-critic method for cooperative multi-agent reinforcement learning," *arXiv preprint arXiv:2104.06655*, May 2021.
- [50] T. Haarnoja, A. Zhou, P. Abbeel, and S. Levine, "Soft actor-critic: Off-policy maximum entropy deep reinforcement learning with a stochastic actor," *arXiv preprint arXiv:1801.01290*, Aug. 2018.
- [51] T. Haarnoja, A. Zhou, K. Hartikainen, G. Tucker, S. Ha, J. Tan, V. Kumar, H. Zhu, A. Gupta, P. Abbeel, and S. Levine, "Soft actor-critic algorithms and applications," *arXiv preprint arXiv:1812.05905*, Jan. 2018.
- [52] H. Sami, A. Mourad, H. Otrok, and J. Bentahar, "Demand-driven deep reinforcement learning for scalable fog and service placement," *IEEE Trans. Serv. Comput.*, vol. 15, no. 5, pp. 2671–2684, Apr. 2022.
- [53] S. Zhang, A. Liu, C. Han, X. Liang, X. Xu, and G. Wang, "Multiagent reinforcement learning-based orbital edge offloading in SAGIN supporting internet of remote things," *IEEE Internet Things J.*, vol. 10, no. 23, pp. 20472–20483, Jun. 2023.
- [54] Y. Zhao, G. Wang, C. Tang, C. Luo, W. Zeng, and Z. Zha, "A battle of network structures: An empirical study of CNN, transformer, and MLP," *arXiv preprint arXiv:2108.13002*, Nov. 2021.
- [55] Y. Yu, J. Tang, J. Huang, X. Zhang, D. K. C. So, and K. Wong, "Multi-objective optimization for UAV-assisted wireless powered IoT networks based on extended DDPG algorithm," *IEEE Trans. Commun.*, vol. 69, no. 9, pp. 6361–6374, Jun. 2021.
- [56] T. Lei, Y. Zhang, S. I. Wang, H. Dai, and Y. Artzi, "Simple recurrent units for highly parallelizable recurrence," *arXiv preprint arXiv:1709.02755*, Sep. 2018.
- [57] X. Shi, Z. Chen, H. Wang, D. Yeung, W. Wong, and W. Woo, "Convolutional LSTM network: A machine learning approach for precipitation nowcasting," *arXiv preprint arXiv:1506.04214*, Aug. 2015.
- [58] J. Chung, Ç. Gülçehre, K. Cho, and Y. Bengio, "Empirical evaluation of gated recurrent neural networks on sequence modeling," *arXiv preprint arXiv:1412.3555*, Aug. 2014.
- [59] Z. Liu, Y. Wang, S. Vaidya, F. Ruehle, J. Halverson, M. Soljacic, T. Y. Hou, and M. Tegmark, "KAN: Kolmogorov-Arnold networks," *arXiv preprint arXiv:2404.19756*, Jun. 2024.
- [60] C. Zhang, G. Sun, J. Li, Q. Wu, J. Wang, D. Niyato, and Y. Liu, "Multi-objective aerial collaborative secure communication optimization via generative diffusion model-enabled deep reinforcement learning," *IEEE Trans. Mob. Comput.*, pp. 1–18, Nov. 2024, early access.
- [61] F. Zhuang, Z. Qi, K. Duan, D. Xi, Y. Zhu, H. Zhu, H. Xiong, and Q. He, "A comprehensive survey on transfer learning," *Proc. IEEE*, vol. 109, no. 1, pp. 43–76, Jul. 2021.
- [62] Y. He, Y. Gan, H. Cui, and M. Guizani, "Fairness-based 3-D multi-UAV trajectory optimization in multi-UAV-assisted MEC system," *IEEE Internet Things J.*, vol. 10, no. 13, pp. 11383–11395, Oct. 2023.
- [63] T. Zhang, K. Zhu, S. Zheng, D. Niyato, and N. C. Luong, "Trajectory design and power control for joint radar and communication enabled multi-UAV cooperative detection systems," *IEEE Trans. Commun.*, vol. 71, no. 1, pp. 158–172, Oct. 2023.

- [64] Z. Wang, B. Lin, Q. Ye, Y. Fang, and X. Han, "Joint computation offloading and resource allocation for maritime MEC with energy harvesting," *IEEE Internet Things J.*, vol. 11, no. 11, pp. 19 898–19 913, Jun. 2024.
- [65] M. Hua and Q. Wu, "Throughput maximization for IRS-aided MIMO FD-WPCN with non-linear EH model," *IEEE J. Sel. Top. Signal Process.*, vol. 16, no. 5, pp. 918–932, May 2022.
- [66] L. He, G. Sun, Z. Sun, J. Wang, H. Du, D. Niyato, J. Liu, and V. C. M. Leung, "Space-air-ground integrated MEC-assisted industrial cyber-physical systems: An online decentralized optimization approach," *arXiv preprint arXiv:2411.09712*, Nov. 2024.
- [67] T. P. Lillicrap, J. J. Hunt, A. Pritzel, N. Heess, T. Erez, Y. Tassa, D. Silver, and D. Wierstra, "Continuous control with deep reinforcement learning," *arXiv preprint arXiv:1509.02971*, Sep. 2015.
- [68] S. Fujimoto, H. van Hoof, and D. Meger, "Addressing function approximation error in actor-critic methods," *arXiv preprint arXiv:1802.09477*, Sep 2018.
- [69] J. Schulman, F. Wolski, P. Dhariwal, A. Radford, and O. Klimov, "Proximal policy optimization algorithms," *arXiv preprint arXiv:1707.06347*, Aug 2017.
- [70] R. S. Sutton and A. G. Barto, "Reinforcement learning: An introduction," *IEEE Trans. Neural Networks*, vol. 9, no. 5, pp. 1054–1054, May 1998.